John von Neumann Institute for Computing

Monte Carlo Protein Folding: Simulations of Met-Enkephalin with Solvent-Accessible Area Parameterizations

Hsiao-Ping Hsu, Bernd A. Berg, Peter Grassberger

published in

NIC Symposium 2004, Proceedings,
Dietrich Wolf, Gernot Münster, Manfred Kremer (Editors),
John von Neumann Institute for Computing, Jülich,
NIC Series, Vol. **20**, ISBN 3-00-012372-5, pp. 323-332, 2003.

http://www.fz-juelich.de/nic-series/volume20

Monte Carlo Protein Folding: Simulations of Met-Enkephalin with Solvent-Accessible Area Parameterizations

Hsiao-Ping Hsu[1], **Bernd A. Berg**[2], **and Peter Grassberger**[1]

[1] Complex Systems Research Group, John von Neumann Institute for Computing
Research Centre Jülich, 52425 Jülich, Germany
E-mail: {h.p.hsu, p.grassberger}@fz-juelich.de

[2] Department of Physics, Florida State University, Tallahassee, FL 32306, USA
E-mail: berg@pamd2.csit.fsu.edu

Treating realistically the ambient water is one of the main difficulties in applying Monte Carlo methods to protein folding. The solvent-accessible area method, a popular method for treating water implicitly, is investigated by means of Metropolis simulations of the brain peptide Met-Enkephalin. For the phenomenological energy function ECEPP/2 nine atomic solvation parameter (ASP) sets are studied that had been proposed by previous authors. The simulations are compared with each other, with simulations with a distance dependent electrostatic permittivity $\epsilon(r)$, and with vacuum simulations ($\epsilon = 2$). Parallel tempering and a recently proposed biased Metropolis technique are employed and their performances are evaluated. The measured observables include energy and dihedral probability densities (pds), integrated autocorrelation times, and acceptance rates. Two of the ASP sets turn out to be unsuitable for these simulations. For all other sets, selected configurations are minimized in search of the global energy minima. Unique minima are found for the vacuum and the $\epsilon(r)$ system, but for none of the ASP models. Other observables show a remarkable dependence on the ASPs. In particular, autocorrelation times vary dramatically with the ASP parameters. Three ASP sets have much smaller autocorrelations at 300 K than the vacuum simulations, opening the possibility that simulations can be speeded up vastly by judiciously chosing details of the force field.

1 Introduction

Protein folding is considered as one of the grand challenges in mathematical biology. Actually, there are several different problems related to protein folding. Strictly speaking, one should distinguish between *fold prediction*, i.e. the mapping of the amino acid sequence onto the geometry of the native configuration, and understanding the *pathway* along which the folding proceeds. Another problem is *inverse* fold prediction, i.e. finding an amino acid sequence which will fold into a desired native configuration.

At present there is no hope that any of this problems can be attacked *ab initio*, i.e. by solving the many-body Schrödinger equation. Instead, one first constructs effective potentials ("force fields") which then allow the dynamics of the nuclei to be treated by classical mechanics. The native state is then identified with the state of lowest energy. There are several such force fields in current use, each one with its weaknesses and strengths. It seems fair to say that their precision typically is sufficient for the correct folding of peptides and small proteins, but not for larger ones with, say, more than 50 amino acids. In addition, some force fields make additional simplifications such as keeping bond lengths fixed or even lumping several small atoms into one effective particle.

Given an amino acid sequence and a force field, finding the native state would then seem straightforward, if there were a single local energy minimum. But, alas, energy landscapes for typical proteins are rough, with many local minima, and finding the global one is highly non-trivial. Basically, there are two methods available for this purpose: molecular dynamics and Monte Carlo methods.

In molecular dynamics (MD) one just solves numerically Newton's equations of motion. This has the advantage that one simulates directly the physical folding process, i.e. one obtains directly the dominant folding paths and one gets immediately estimates for the folding times. There are of course many details which can be adjusted to make the simulation faster and more realistic (e.g., one can include thermal noise and solve a Langevin equation, or one can treat Coulomb forces more efficiently), but basically one has not much freedom in putting up the simulations, and these simulations tend to be slow – very slow!

This is in contrast to Monte Carlo (MC) simulations. There one gives up any claim to follow the actual path, but one jumps in phase space as efficiently as possible, subject only to the constraint that one samples configurations according to the Boltzmann-Gibbs distribution, $p(\mathrm{config}) \propto \exp(-E(\mathrm{config})/k_B T)$. Indeed, with modern advanced MC methods one may even give up this requirement and re-weight eventually the final distribution to obtain proper sampling[1–9]. Since one is completely free in how one moves in phase space (one may even move by adding or removing particles, see Ref. 10), such a strategy can be very efficient if the moves are well chosen – but it can also be extremely inefficient, if they are badly chosen.

In nature biomolecules exist in the environment of solvents (i.e. water, in general), thus the molecule-solvent interactions must be taken into account. Indeed, neglecting the ambient water altogether can lead to gross errors. In MD simulations water just slows down the simulations because the number of particles increases by a factor between two and ten. For MC simulations the situation is much worse. For steric reasons, many moves which would be very efficient *in vacuo*, become inefficient (i.e., are accepted with small probabilities) if the molecule is surrounded by water. This is the main reason why chemists in general prefer MD over MC methods.

Since it is so very computer time consuming to simulate proteins when the surrounding water is treated explicitly, a number of approximate treatments of solvent effects have been developed, where the water is treated only *implicitly*. In the *solvent-accessible area approach*[11–13] it is assumed that the protein-solvent interaction is given by the sum of the surface area of each atomic group times a parameter called *atomic solvation parameter* (ASP). The choice of a set of ASPs (also called hydrophobicity parameters or simply hydrophobicities) defines a model of solvation. However, there is no agreement on how to determine the universally best set of ASPs, or at least the best set for some limited purpose. For instance, eight sets were reviewed and studied by Juffer et al.[14] and it was found that they give rather distinct contributions to the free energy.

In Ref. 15 we investigated how different ASP sets modify the Metropolis simulations of the small brain peptide Met-Enkephalin (Tyr-Gly-Gly-Phe-Met) at 300 K. The reason for the choice of Met-Enkephalin is that its vacuum properties define a reference system for testing numerical methods, e.g. Ref. 1–5, 9. Therefore, Met-Enkephalin appears to be well suited to set references for the inclusion of solvent effects as well, but we are only aware of few articles[16, 17], which comment on the modifications due to including a solvent model. On the other hand, the effect of ASP models on the helix-coil transition of polyalanine has

been studied recently[18].

The simulation temperature was chosen as 300 K in Ref. 15, because room temperature is the physical temperature at which biological activity takes place. Most of the previous simulations of Met-Enkephalin in vacuum were performed at much lower temperatures or employed elaborate minimization techniques with the aim to determine the global energy minimum (GEM). Only recently[9] it was shown that the GEM is well accessible by local minimization of properly selected configurations from an equilibrium time series at 300 K. Precisely this should be the case for a GEM which is of relevance at physical temperatures.

For our simulations we use the program package SMMP[19] (Simple Molecular Mechanics for Proteins) together with parallel tempering[20–22] (PT) and the recently introduced[9] biased Metropolis technique RM_1 (rugged Metropolis – approximation 1). SMMP implements a number of all-atom energy functions, describing the intramolecular interactions, and nine ASP sets[13,23–29] to model the molecule solvent interactions. We use the ECEPP/2[30] (Empirical Conformational Energy Program for Peptides) energy function with fully variable ω angles and simulate all nine ASP sets. For comparison we simulate also Met-Enkephalin in vacuum and with the distance dependent electrostatic permittivity $\epsilon(r)$ of Ref. 31.

The energy functions and some details of the Metropolis methods used are explained in Sec. 2. In Sec. 3 we present the main results. Summary and conclusions are given in Sec. 4.

2 Models and Methods

2.1 Force Field and Atomic Solvation Parameter Sets

In all-atom models of biomolecules the total conformational energy of the intramolecular interactions E_I is given as the sum of the electrostatic, the Lennard-Jones (Van der Waals), the hydrogen bond, and the torsional contributions,

$$E_I \;=\; 332 \sum_{i<j} \frac{q_i q_j}{\epsilon r_{ij}} \;+\; \sum_{i<j} \left(\frac{A_{ij}^{\mathrm{LJ}}}{r_{ij}^{12}} - \frac{B_{ij}^{\mathrm{LJ}}}{r_{ij}^{6}} \right) \;+$$
$$\sum_{i<j} \left(\frac{A_{ij}^{\mathrm{HB}}}{r_{ij}^{12}} - \frac{B_{ij}^{\mathrm{HB}}}{r_{ij}^{10}} \right) \;+\; \sum_{k} U_k \left[1 \pm \cos(n_k \phi_k) \right] . \qquad (1)$$

Here r_{ij} is the distance between atoms i and j, q_i and q_j are the partial charges on the atoms i and j, ϵ is the electric permittivity of the environment, A_{ij}, B_{ij}, C_{ij} and D_{ij} are parameters that define the well depth and width for a given Lennard-Jones or hydrogen bond interaction, and ϕ_k is the k-th torsion angle. The units are as follows: distances are in Å, charges are in units of the electronic charge and energies are in kcal/mol.

One of the simplest ways to include interactions with water is to assume a distance dependent electrostatic permittivity according to the formula[31,32]

$$\epsilon(r) = D - \frac{D-2}{2} \left[(sr)^2 + 2sr + 2 \right] e^{-sr} . \qquad (2)$$

Empirical values for the parameters D and s are chosen so that the permittivity takes the value of bulk water, $\epsilon = 80$, for large distances, and the value $\epsilon = 2$ for small r, i.e. for

the interior of the molecule. This approach is clearly an oversimplification, because atoms which are close to each other do not necessarily have to be simultaneously in the interior of the molecule. Reversely, two atoms which are separated by a large distance may still be in the interior of the molecule. More elaborated approaches are asked for.

If the molecule-solvent interaction is proportional to the surface area of the atomic groups, it is given by the sum of contributions of a product of the surface area of each atomic group and the atomic solvation parameter[13],

$$E_{\rm sol} = \sum_i \sigma_i A_i \, . \tag{3}$$

Here $E_{\rm sol}$ is the solvation energy and the sum is over all atomic groups. A_i is the solvent accessible surface area and σ_i the atomic solvation parameter of group i. The choice of a set of ASPs σ_i defines a model of solvation. In our work, we used the same nine sets of ASPs as in the SMMP package and refer to[19,15] for notations and details.

2.2 Metropolis Methods

For the updating we used PT with two processors, one running at 300 K and the other at 400 K. This builds on the experience[9] with vacuum simulations of Met-Enkephalin for which the following observations are made:

1. The integrated autocorrelation time $\tau_{\rm int}$ (defined below in this section) increases from 400 K to 300 K by a factor of ten for the (internal) energy and by factors of more than twenty for certain dihedral angles.

2. The energy probability densities (pds) at 300 K and 400 K overlap sufficiently, so that the PT method works, leading to an improvement factor of about 2.5 in the real time needed for the simulation (see Table I of Ref. 9).

A detailed description of the PT algorithm is given in Ref. 15. It used an approximation, called RM_1, to the rugged Metropolis scheme introduced in Ref. 9 which had given an improvement by an additional factor of two for the vacuum system[9]. Finally, the GEM was determined by minimizing selected configurations of the 300 K time series. More precisely,

1. We determined the lower 10% quantile $E_{0.1}$ and the upper 10% quantile $E_{0.9}$ of the energy distribution of our time series. This is done by sorting all energies in increasing order and finding the values which cut out the lower and upper 10% of the data. For the statistical concepts see, e.g., Ref. 36.

2. We partitioned the time series into bunches of configurations. A bunch contains the configurations from one crossing of the upper quantile $E_{0.9}$ to the next so that at least on crossing of the lower quantile $E_{0.1}$ is located between the two crossings of $E_{0.9}$. For each bunch we picked then its configuration of lowest energy. The idea behind this procedure is to pick minima of the time series, which are to a large degree statistically independent.

3. We run a conjugate gradient minimizer on all the selected configurations and thus obtain a set of configurations which are local energy minima. For the vacuum simulation[9] about 5% to 6% of the thus minimized configurations agreed with the GEM.

To determine the speed at which the systems equilibrate, we measured the integrated autocorrelation time $\tau_{\rm int}$ for the energy and each dihedral angle. These times are directly proportional to the computer run times needed to achieve the same statistical accuracy for each system. They thus determine the relative performance of distinct algorithms. For an observable f the autocorrelations are

$$C(t) = \langle f_0\, f_t \rangle - \langle f \rangle^2, \tag{4}$$

where t labels the computer time. Defining $c(t) = C(t)/C(0)$, the time-dependent integrated autocorrelation time is given by

$$\tau_{\rm int}(t) = 1 + 2 \sum_{t'=1}^{t} c(t') \; . \tag{5}$$

Formally the integrated autocorrelation time $\tau_{\rm int}$ is defined by $\tau_{\rm int} = \lim_{t\to\infty} \tau_{\rm int}(t)$. Numerically, however, this limit cannot be reached as the noise of the estimator increases faster than the signal. Nevertheless, one can calculate reliable estimates by reaching a window of t values for which $\tau_{\rm int}(t)$ becomes flat, while its error bars are still reasonably small. The data given in the next section were obtained in this way, see Ref. 37 for a more detailed discussion.

3 Results

3.1 Autocorrelations

The PT simulations with temperatures $T_0 = 400\,\mathrm{K}$ and $T_1 = 300\,\mathrm{K}$ are performed on the system in vacuum ($\epsilon = 2$), with $\epsilon(r)$ given by Eq. (2) and for the nine ASP sets in the SMMP package. The ranges of the dihedral angles are not restricted but vary in the full range from $-\pi$ to π. Each measurement is based on $\approx 2 \times 10^6$ sweeps, where one sweep is defined by updating each dihedral angle once. On the Cray T3E, this takes about 14 hours for the vacuum system and 5×14 hours for each ASP set.

Results of the time-dependent integrated autocorrelations times (5) for the vacuum simulations and the ASP sets OONS and EM86 are shown in Fig. 1a. In each case a window of t values is reached for which $\tau_{\rm int}(t)$ does no longer increase within its statistical errors. In the case of the vacuum simulations it even decreases, but this is not significant due to the statistical error. These windows are then used to estimate the asymptotic $\tau_{\rm int}$ for all ASP sets except the ASP sets JRF and BM.

The acceptance rates of the solvent models JRF and BM are much lower than for the other models. In essence the simulations of these two models get stuck, which implies that their integrated autocorrelation times cannot be measured. The pds of the dihedral angles of these two models are also erratic and the conclusion is that they cannot be used to describe Met-Enkephalin in solvent.

The energy couples to all dihedral angles and its integrated autocorrelation time is characteristic for the entire system, while the integrated autocorrelation times of the single dihedral angles vary heavily from angle to angle. For all systems but JRF and BM, we show in Fig. 1b the integrated autocorrelation times at 300 K for the energy and all dihedral angles. The notation v_i, $i = 0, 1, \ldots, 24$ is used, where v_0 is stands in for the energy E and for $i = 1, \ldots, 24$.

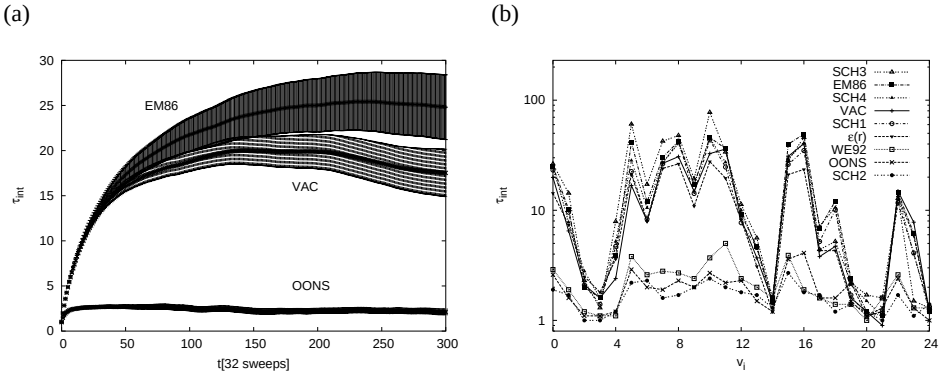

Figure 1. (a) The time-dependent integrated autocorrelation time for the energy at 300 K from our simulations of the vacuum system and the solvent models EM86 and OONS. (b) Integrated autocorrelation times for the energies ($v_0 = E$) and the dihedral angles v_i, $i = 1, \ldots, 24$ at $T = 300$ K.

In Fig. 1b we see that for each dihedral angle v_i the integrated autocorrelation times $\tau_{\mathrm{int}}[v_i]$ for the three solvent models OONS, WE92 and SCH2 are smaller than for the remaining systems, including the vacuum system. In particular, this means that the OONS, WE92 and SCH2 models require far less statistics than the vacuum run for achieving the same accuracy of results. In the following the solvation models OONS, WE92 and SCH2 define the "fast class", while the other models shown in Fig. 1b constitute the "slow class" (the models JRF and BM are omitted from this classification). "Good" behavior of the models OONS and WE92 has been previously observed[38]. Precise values of the autocorrelation times and further details on their measurements can be found in Ref. 15.

3.2 Structure

For all our simulations we applied the method outlined in subsection 2.2 to determine local energy minima. Again, the results of the JRF and BM solvent model are erratic. The BM model is entirely frozen, only $N_{\mathrm{conf}} = 2$ different configurations are ever reached at 400 K and $N_{\mathrm{conf}} = 1$ at 300 K. Therefore, we do not give minimization results for BM. For JRF the N_{conf} numbers are more reasonable, but still by a factor of one third and less smaller than the N_{conf} numbers of each other system. JRF is also disregarded in the following discussion.

Only if the same energy minimum is hit $N_{\mathrm{hits}} > 1$ times, we can argue that we found the GEM. This was the case for the vacuum and for the $\epsilon(r)$ simulations (notably already at 400 K), but not for any of the ASP solvent models. There, each minimization led to a different state. This is a very interesting observation, as it might indicate that the energy landscape is rougher for the ASP solvent models. But if this were the case, we should also expect that autocorrelations are longer for the ASP solvent models, while the opposite was found at least for three ASP parameter sets.

Indeed we were not the first to observe this phenomenon. Quite some time ago Li and Scheraga[1,16] developed a Monte Carlo minimization method and applied it to Met-Enkephalin in vacuum and in solvent modeled by OONS. While for the vacuum system

their method converged consistently to the GEM, all their five runs of the solvent model led to different conformations with comparable energies. They interpreted their results in the sense that Met-Enkephalin in water at 20°C is presumably in an unfolded state for which a large ensemble of distinct conformations co-exist in equilibrium. A consistent scenario was later observed in NMR experiments[39].

Although the minimization method of Li and Scheraga is entirely different from ours, they essentially tested for valleys of attraction to the GEM at room temperature, quite as we do in the present paper. So, we have not only confirmed their old result, but find that it is common to a large set of ASP models implemented in SMMP. Neither the method by which an ASP set was derived, nor whether it belongs to the fast or slow class, appears to matter with this respect.

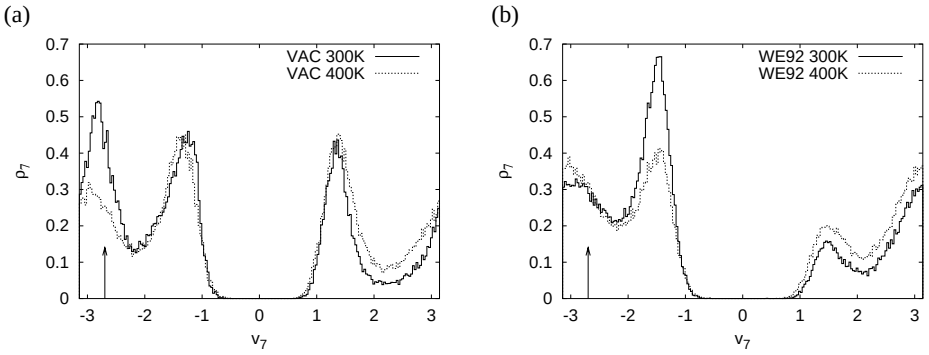

Figure 2. Probability densities of the dihedral angle v_7 for (a) the vacuum simulation and (b) the WE92 simulation. The arrow indicates the vacuum GEM value of this angle.

In a search for structural differences of Met-Enkephalin in the different models, we looked at the pds of the dihedral angles. For all systems and both temperatures there are altogether $2 \times 9 \times 24 = 432$ distributions. At the first look the pds of the different systems are amazingly similar, independently of whether they are from systems of the fast or slow class, from an ASP model, from the vacuum or from the $\epsilon(r)$ simulation. A more careful investigation reveals differences which appear to relate to the distinct behavior under our minimization. For the dihedral angle v_7 this is illustrated in Fig. 2a and Fig. 2b. Its probability densities are compared at 300 K and 400 K. For the vacuum simulation the pds are depicted in Fig. 2a and from 400 K to 300 K we observe an increase of the peak close to the arrow which indicates the vacuum GEM value of v_7. In contrast to this, the wrong peak increases for the WE92 solvent model (Fig. 2b).

One may suspect that the difference between the models of our fast and slow classes is simply due to an effectively higher temperature for the three models of the fast class. To gain insight into this question, we calculate the corresponding entropies. Each pd is discretized as a histogram of 200 bins, ρ_{ij}, where $i = 1, \ldots, 24$ labels the dihedral angles,

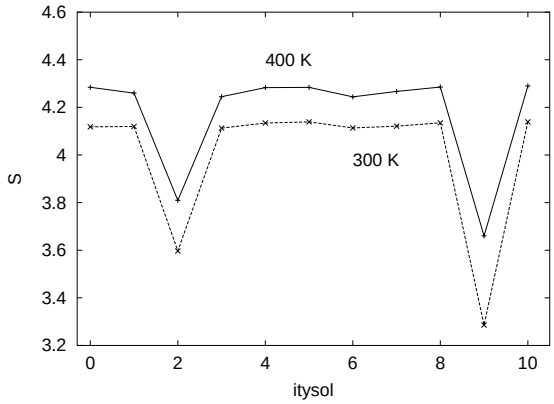

Figure 3. Overall entropies of the dihedral angles. The numbers on the x-axis label the different models, with `itysol` $= 0$ for vacuum and `itysol` $= 10$ for the $\epsilon(r)$ model.

and $\sum_{j=1}^{200} \rho_{ij} = 1$. The entropy of a dihedral angle is then defined by

$$S_i = -\sum_{j=1}^{200} \rho_{ij} \, \ln \rho_{ij} \tag{6}$$

and the total entropy of the pds of an ASP model is $S = \sum_i S_i$. In Fig.3 these entropies are depicted for all our models. The lines between the data points are just drawn to guide the eyes. The dips for the JRF and the BM model show, again, that their configurations are essentially frozen. For the other models we see a decrease of entropy from 400 K to 300 K, but we find no larger entropy for the models of the fast class than for the models of the slow class. Therefore, the effective temperature scenario is ruled out. Instead, it seems that for the models of the fast class the solvent has some kind of "lubrication" effect, which accelerates the simulation.

Strong similarities between the ASP models of the fast class on one side and the ASP models of the slow class on the other side are found for the solvation energies, the gyration radii and the end-to-end distances.

4 Summary and Conclusions

We have reported on simulations of Met-Enkephalin at room temperature (300 K) for nine different solvation models. Quantitative results obtained in that way should not be trusted, because the methods to derive the ASPs have been quite crude. Also our simulations do not give information that would allow us to pick a best ASP set for the intended purpose of simulating Met-Enkephalin at 300 K. Nevertheless, we obtained a number of very interesting consequences which should be more general and which should apply to any attempt to include solvation effects in Monte Carlo calculations.

If we exclude two ASP sets which behave erratic (at least as implemented in SMMP[19]), we have still nine models: seven ASP sets, vacuum simulations with $\epsilon = 2$, and the $\epsilon(r)$

system[31]. These models seperate into a fast and a slow class with respect to their autocorrelation times. Vacuum simulations are in the slow class. This leads to the interesting feature that it takes less computer time to estimate physical observables at room temperature in the fast solvation models OONS[23], WE92[27], and SCH2[25,28] than it takes for vacuum, despite the substantial increase of the computer time per sweep by a factor of about 5 for the solvation models over the vacuum system. We have no clear clue why some models have a fast and others a slow dynamics. But the possibility that slightly different force fields can lead to vastly different autocorrelation times is of course something which should be kept in mind.

We applied the minimization procedure of Ref. 9 in an attempt to locate the GEM for the nine systems which are reasonably well-behaved under Metropolis simulations at 300 K. The GEM is unambiguously found for the vacuum system and for the simulation with a distance dependent electrostatic permittivity. No true GEM is found for any of the remaining seven ASP models. This confirms an old result of Li and Scheraga[16], who concluded that at room temperature Met-Enkephalin in water is likely in an unfolded state. To get a better understanding of this result, we studied at 300 K the dihedral pds in some details. At a first glance they look quite similar for all the models in the fast as well as in the slow class. Differences are found for a number of details, which may allow to explain why the 300 K configurations of the ASP models behave entirely different under our minimization procedure than the vacuum and the $\epsilon(r)$ systems.

The central question, which remains to be settled, is whether ASP models will ultimately allow for accurate Metropolis simulations of biomolecules like Met-Enkephalin in solvent or not. In principle, this could be decided by comparing with simulations with explicit solvent, but this has not yet been done.

5 Acknoledgements

The computer simulations were carried out on the Cray T3E of the John von Neumann Institute for Computing. BB acknowledges partial support by the U.S. Department of Energy under contract No. DE-FG02-97ER41022.

References

1. Z. Li and H.A. Scheraga, Proc. Nat. Acad. Sci. USA, **85**, 6611 (1987).
2. Y. Okamoto, T. Kikuchi, and H. Kawai, Chem. Lett. **1992**, 1275 (1992).
3. U.H. Hansmann and Y. Okamoto, J. Comp. Chem. **14**, 1333 (1993).
4. H. Meirovitch, E. Meirovitch, A.G. Michel, and M. Vásquez, J. Phys. Chem. **98**, 6241 (1994).
5. U.H. Hansmann, Y. Okamoto, and J.N. Onuchic, PROTEINS: Structure, Function, and Genetics **34**, 472 (1999).
6. Y. Okamoto, e-print cond-mat/0308360 (2003).
7. T. Wille and U.H.E. Hansmann, Phys. Rev. Lett. **88**, 068105 (2002).
8. F. Wang and D.P. Landau, Phys. Rev. E **64**, 056101 (2001).
9. B.A. Berg Phys. Rev. Lett. **90**, 180601 (2003).
10. P. Grassberger, *Sequential Monte Carlo Methods for Protein Folding*, these proceedings.

11. B. Lee and M. Richards, J. Mol. Biol. **55**, 379 (1971).
12. C. Cothia, Nature **248**, 338 (1974).
13. D. Eisenberg, A.D. McLachlan, Nature **319**, 199 (1986).
14. A.H. Juffer, F. Eisenhaber, S.J. Hubbard, D. Walther, P. Argos, Protein Sci. **4**, 2499 (1995).
15. B.A. Berg and H.-P. Hsu, e-print cond-mat/0306435 (2003).
16. Z. Li and H.A. Scheraga, J. Mol. Struct. (Theochem) **179**, 333 (1988).
17. M. Kinoshita, Y. Okamoto, and F. Hirata, J. Am. Chem. Soc. **120**, 1855–1863 (1998).
18. Y. Peng, U.H. Hansmann, and N.A. Alves, J. Chem. Phys. **118**, 2374 (2003); Y. Peng and U.H. Hansmann, Biophys. J. **82**, 3269 (2003).
19. F. Eisenmenger, U.H. Hansmann, S. Hayryan, and C.-K. Hu, Comp. Phys. Commun. **138**, 192 (2001).
20. G.J. Geyer, in *Computing Science and Statistics*, Proceedings of the 23rd Symposium on the Interface, E.M. Keramidis (editor), Interface Foundation, Fairfax, Virginia, 1991, pp.156–163.
21. K. Hukusima and K. Nemoto, J. Phys. Soc. Japan **65**, 1604 (1996).
22. U.H. Hansmann, Chem. Phys. Lett. **281** 140 (1997).
23. T. Ooi, M. Obatake, G. Nemethy, and H.A. Scheraga, Proc. Natl. Acad. Sci. USA **84**, 3086 (1987).
24. D. Eisenberg, M. Wesson, M. Yamashita, Chem. Scrip. **A 29**, 217 (1989).
25. A. Kim, *Amino acid side chain contributions to free energy of transfer of tripeptides from water to octanol*, dissertation, University of California at San Francisco, 1990.
26. J. Vila, R. L. Williams, M. Vásquez, H. A. Scheraga, Proteins Struct. Funct. Genet. **10** 199 (1991).
27. L Wesson, D. Eisenberg, Protein Sci, **1**, 227 (1992).
28. C. A. Schiffer, J. W. Caldwell, P.A. Kollman, and R. M. Stroud, Mol. Simul. **10**, 121 (1993).
29. B. von Freyberg, T. J. Richmond, and W. Braun, J. Mol. Biol. 233, 275 (1993).
30. M.J. Sippl, G. Nemethy, and H.A. Scheraga, J. Phys. Chem. **88**, 6231 (1984) and references given therein.
31. B. Hingerty, R.H. Richie, T.L. Ferrel, and J. Turner, Biopolymers **25**, 427 (1985).
32. Y. Okamoto, Biopolymers **34**, 529 (1994).
33. J.L. Fauchere and V. Pliska, Eur. J. Med. Chem. Chim. Ther. **18**, 369 (1983).
34. S. Cabani, P. Gianni, V. Mollica, and L. Lepori, J. Solution Chem. **10**, 563 (1981).
35. R. Wolfenden, L. Andersson, P.M. Cullis, and C.C.B. Southgate, Biochemistry **20**, 849 (1981).
36. S. Brandt, *Statistical and Computational Methods in Data Analysis* (North-Holland Publishing Company, Amsterdam, 1983).
37. A. Sokal, in *Functional Integration: Basics and Applications*, C. DeWitt-Morette, P. Cartier and A. Folacci (editors), Cargese Summer School, Plenum Press, New York, 1997, pp.131–192.
38. M. Masuya and Y. Okamoto, quoted in Y. Okamoto, Rec. Res. Dev. in Pure & Appl. Chem. **2**, 1 (1998).
39. W.H. Graham, E.S. Carter II, and R.P. Hicks, Biopolymers **32**, 1755 (1992).